ISBN: 978-3-95450-249-3 ISSN: 2673-5350 doi: 10.18429/JACoW-IBIC2024-TUP57

HETERODYNE NEAR-FIELD SPECKLE SIMULATIONS USING SRW AT THE ALBA FE21

U. Iriso*, J.M. Alvarez, A. Nosych, J. Núñez,
E. Solano, L. Torino, ALBA-CELLS, Cerdanyola del Vallès, Spain
B. Paroli, M. A. C. Potenza, M. Siano, Università degli Studi di Milano, Milan, Italy
D. Butti, S. Mazzoni, G. Trad, CERN, Geneva, Switzerland

Abstract

Several experiments were done to measure the transverse beam size at the NCD ALBA beamline using the Heterodyne Near Field Speckles (HNFS) technique. Inside the FCC collaboration, it was decided to move these experiments to the ALBA Front End 21, where currently an x-ray pinhole camera is working since 2021. The goal is that the two measurement techniques can work alternatively and measure the electron beamsize of the same source point, so that a direct comparison between both techniques can be done. This paper reports the SRW simulations performed in order to investigate the feasibility of the HNFS experiments at this new location. In particular, it focuses on the effect of the dipole radiation and the design of the high energy and high bandwidth monochromator required to perform HNFS experiments at this location.

INTRODUCTION

During standard operation, the transverse beam profile of the electron beam at ALBA Synchrotron is measured via the X-ray pinhole camera technique [1]. This direct imaging technique allows a fast rendering of the transverse profile but presents a limited beam-size resolution due to diffraction effects. Amongst other options, the X-ray Heterodyne Near Field Speckle technique (XHNFS) promises to solve this issue and also provides an effective measurement of the spatial coherence properties of the radiation beam.

The XHNFS method is based on the interference between the weak spherical wavefronts scattered by small obstacles (with size in the sub-μm range, in our case a water-based suspension of colloidal particles) and the intense transmitted X-ray beam. This interference is called "speckle" pattern. From the Fourier analysis of the speckle pattern, we measure the coherence length, which ultimately allows to measure the source (electron) beam size. This method has been already tested at the NCD-Sweet ALBA Beamline [2], but also at other labs [3, 4].

This method is one of the candidates to measure the beam size at the Future Circular Collider (FCC) [5]. As part of the FCC collaboration between ALBA, CERN, and the University of Milano, and with the goal of properly calibrate this technique, it was decided to move these experiments to the ALBA Front End 21 (FE21), where an x-ray pinhole camera is working since 2021 [1]. The goal is that the two measurement techniques can work alternatively and measure the electron beam size of the same source point, so that a direct comparison between both techniques can be done.

The sketch of the FE21 is shown in Fig. 1, with components (already installed) for the x-ray pinhole and the required XHNFS components currently under design. The black elements show the fixed components, whereas the components in green need to be designed. Using remote control motors, either pinhole measurements or XHNFS measurements can be taken alternatively.

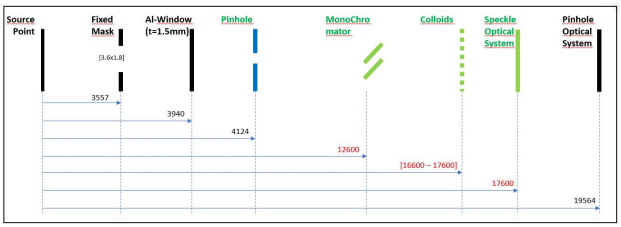

Figure 1: Sketch of FE21, with the elements of the x-ray pinhole and the components that need to be designed for the XHNFS (in green).

Note that FE21 is equipped with an Al-window with a thickiness of 1.5 mm, which filters out the soft x-rays for the pinhole camera. Although this radiation is enough to produce a good image using the pinhole technique, it might not be enough for the XHNFS experiments. Actually, Fig. 2 compares the flux produced by the In-Vacuum Undulator at the NCD beamline (red) with the flux produced by the bending dipole at FE21 (blue). The green trace shows the flux remaining after the Al-window in the FE21. Note that there is around 2-3 orders of magnitude difference. Therefore the design of the XHNFS experiments needs to optimize as much as possible the flux impinging on the detection system.

In order to increase the flux arriving at the sample, we look for a high bandwidth monochromator allowing more intensity to pass through the optical system and onto the detection screen. However, in this case, the effects of temporal coherence might start to be noticeable reducing the visibility of the interference fringes. Thus, the goal of this work is to find the appropriate monochromator bandwidth, providing a good trade-off between 1) the high flux at the detection system (to properly see the speckle interference pattern) and 2) the speckle pattern is not affected by the temporal coherence due to the large bandwidth. These effects have been simulated using the code Synchrotron Radiation Workshop - SRW [6].

* uiriso@cells.es

ISBN: 978-3-95450-249-3 ISSN: 2673-5350 doi: 10.18429/JACoW-IBIC2024-TUP57

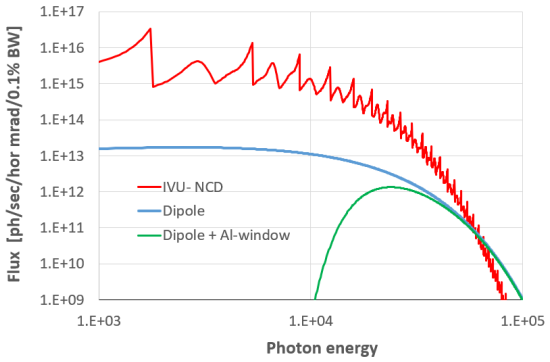

Figure 2: Flux for the In-Vacuum Undulator at the NCD beamline compared with the dipole flux at FE21. The green trace marks the remaining flux after the 1.5 mm Al-window in FE21, whose peak is at 23.7 keV.

Table 1: FE21 Parameters used for SRW Simulations

Parameter	Value
beam energy	3 GeV
dipole field	1.42 T
dipole length	1.4 m
dipole bending radius	7.04 m
x-ray energy peak	23.7 keV
Monochromator bandwidth	10^{-4} - 10^{-1}
horizontal beamsize	60 µm
vertical beamsize	30 µm
horizontal divergence	5 µrad
vertical divergence	2 µrad
Energy spread	0.001

SRW SIMULATIONS AT FE21

The geometrical system depicted in Fig. 1 is reproduced in SRW. After the bending magnet, the first optical elemement is a fixed mask with an aperture of (3.6×1.8) mm. Then, the radiation passes through an Al-window, a monochromator and through the colloid system, to finally end up in the detection screen. The colloid system is taken as the one in our old studies [2], a water suspension of SiO_2 nanospheres whose diameter is 500 nm. Table 1 shows the beam parameters used as input for the SRW simulations.

In order to avoid very large time-consuming simulations, our wavefront is cut by a about a factor 10 with respect to the fixed mask aperture ~(0.4x0.2)mm. This produces slight diffraction effects at the borders of the wavefront, whereas the interference patterns concentrating in the centre remain unperturbed. Furthermore, we also found that meaningful results are obtained sampling the electron beam with (only) 500 particles. This means that we ran our programme for 500 loops, changing in each one the position and momentum of the initial electron generating the X-rays, and then we sum the resulting intensity distributions. This way, using parallel processing and the ALBA HPC Cluster, a full simulation (for one single wavelength) lasts ~ 5 hours.

We further speed-up the CPU time by running simulations for a single nanosphere only, as the 2D FFT of one single colloid produces the same results of multiple scatterers [2, 7]. This stems from the heterodyne regime of the XHNFS technique, allowing to decompose the speckle pattern $s(\vec{x})$ at a distance z into the intensity (incoherent) sum of many equal single-colloid interference images $i(\vec{x}, z)$ [8]:

$$s(\vec{x}, z) = \sum_{j=1}^{N} i_j(\vec{x}, z) \,, \tag{1}$$

Using the linearity of the Fourier transform operation [9]:

$$\hat{s}(\vec{q}, z) = \sum_{j=1}^{N} \hat{i}_j(\vec{q}, z) \,, \tag{2}$$

where $\hat{s} = FT\{s\}$ and $\hat{i}_j = FT\{i_j\}$.

By taking the squared modulus of Eq. (2), we obtain the following convenient form for the power spectrum $PS(\vec{q}, z)$ of the speckle patterns at a distance z:

$$PS(\vec{q}, z) = \sum_{j=1}^{N} |\hat{s}_j(\vec{q}, z)|^2 + \sum_{j \neq k} \hat{s}_j(\vec{q}, z)\hat{s}_k^*(\vec{q}, z) \,, \tag{3}$$

Finally, by the shift theorem of the Fourier transform operation [9], the random positions of the colloidal particles in the suspension are transformed into pure random phase factors in the Fourier transform of the single-particle interference images. Therefore, the first term in Eq. (3) reduces to $N \cdot I(\vec{q}, z)$, where $I(\vec{q}, z) = |\hat{s}(\vec{q}, z)|^2$ is the power spectrum of the single-colloid interference image, whereas the second term averages to zero. As a result, under heterodyne conditions the power spectrum of the single-colloid interference pattern yields the same result as the power spectrum of the actual speckles (from many colloids), apart for inessential multiplicative factors [8].

Figure 3 (left) shows the interference pattern produced by a single colloid using the beam parameters in Table 1 for a monochromatic beam of 23.7 keV. The right hand side picture shows the 2D power spectrum of it. Although the intensity fringes in Fig. 3 (left) may seem a bit blurry, the Fourier transform in Fig. 3 (right) shows that both the horizontal and vertical profiles follow very well the theoretical predictions. This is shown in Fig. 4, where the horizontal (top) and vertical (bottom projection given by SRW (in blue) are very well fitted with the theoretical model of the so-called Talbot oscillations (pink) [2]:

$$I(q, z) = T(q, z)S(q) \left| \mu \left(z\frac{\vec{q}}{k} \right) \right|^2 , \tag{4}$$

where q is the spatial frequency, defined as $q = kr/z$ with $\vec{r} = (x, y)$ being the vector at the detection plane, z the distance between the colloids and the screen, and $k = 2\pi/\lambda$. The function $T(q, z) = 2\sin^2 \frac{zq^2}{2k}$ is the Talbot transfer function, $S(q)$ is the particle form factor, and μ represents the Complex Coherence Factor. More details about these formulae can be found in [2].

ISBN: 978-3-95450-249-3 ISSN: 2673-5350 doi: 10.18429/JACoW-IBIC2024-TUP57

We note that the small perturbations in the horizontal fit (around q=±3) are due to numerical artefacts. In fact, we saw that by reducing the mesh size these artefacts go away. Most importantly, they do not intefere with the central part of the Fourier transform, from where the physical parameters are inferred. With these parameters, we reproduce an horizontal and vertical beam size of (59.2, 30.5) µm, which are very close to the original parameters in Table 1.

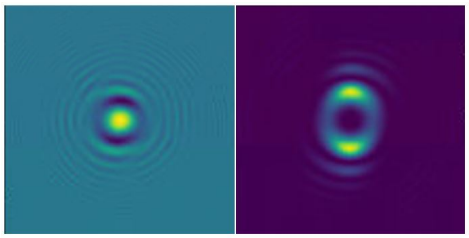

Figure 3: Speckle pattern of one single-colloid (left) and 2D FFT of it (right). The simulation corresponds to a perfectly monochromatic x-ray beam of E_0=23.7 keV.

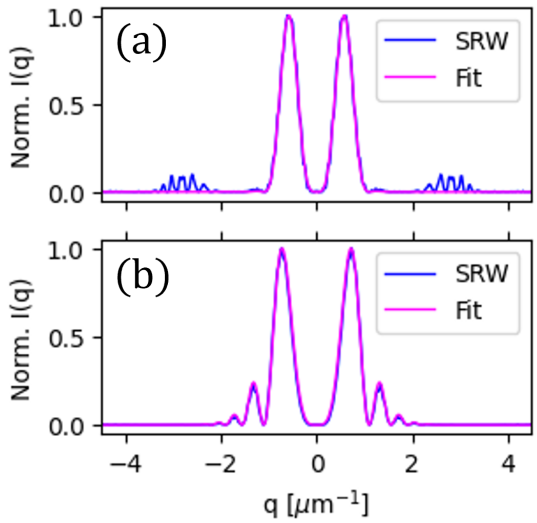

Figure 4: Theoretical fits with Eq. (4) of the horizontal (a) and vertical (b) profiles of the Fourier transform of the intensity distribution simulated with SRW. The fit parameters were the measured beam sizes $\hat{\sigma}_H$ = 59.2 µm and $\hat{\sigma}_V$ = 30.5 µm.

ENERGY BANDWIDTH STUDIES

In order to evaluate the effect of the monochromator bandwidth, we repeat the simulations in the previous section for different wavelengths, adding them up according to the reflectivity curve of the monochromator. Typical Si(111) monochromators, as the one used in our previous experiments [2], have a bandwidth of 10^{-4}. Here we simulate monochromators having Gaussian reflectivity curves with rms of $\Delta E/E$=10^{-3}, 10^{-2} and 10^{-1}. Our goal is to have a similar flux as the one in our previous experiments in the NCD beamline, while at the same time minimizing the effects of temporal coherence.

To this aim, we look at the error in the retrieved beam size produced by the different monochromator bandwidhts. That is, the difference between the horizontal and vertical beamsizes obtained after the analysis of the speckle pattern $\sigma_{x,M}$ for a given bandwidth, with respect to the theoretical beamsizes $\sigma_{x,0}$ in Table 1: that is, $(\sigma_{x,M} - \sigma_x^0)/\sigma_{x,0}$. This is what is shown in Fig. 5, which shows the error for both the vertical and horizontal directions at different bandwidths and its corresponding flux. The flux at NCD is shown in a red dashed line for reference. This demonstrates that our monochromator should have a bandwidth in the order of 10^{-2} to have meaningful results and still keep a flux similar to the one at NCD.

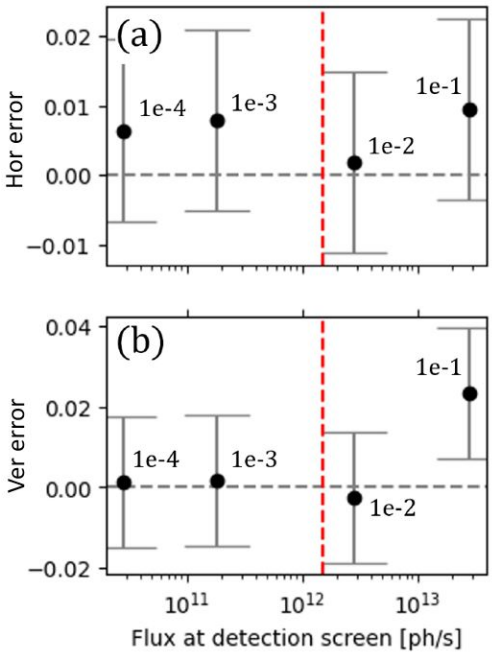

Figure 5: Computed beam size error for different monochromator bandwidths for the horizontal (a) and vertical (b) planes. For reference, the vertical red dashed line shows the flux at the NCD beamline.

MONOCHROMATOR: TECHNICAL CHOICES

After the studies in the previous section, we look for a monochromator with an energy peak at E_0=23.7 keV, with an energy bandwidth of $\Delta E/E$=1%. Increasing the bandwidth of a monochromator is achieved by adding several multilayers to a Si substrate. In this case, several bi-layer options were studied: W/B4C or W/Si, with a thickness ranging between 2.0 and 2.4 nm/bilayer. A comparison of both materials is shown in Fig. 6: in both cases, the reflectivity R at the peak energy of 23.7 keV is R~0.85 and the bandwidth is around 1.2‰, being slightly larger the bandwidth of W/Si.

ISBN: 978-3-95450-249-3 ISSN: 2673-5350 doi: 10.18429/JACoW-IBIC2024-TUP57

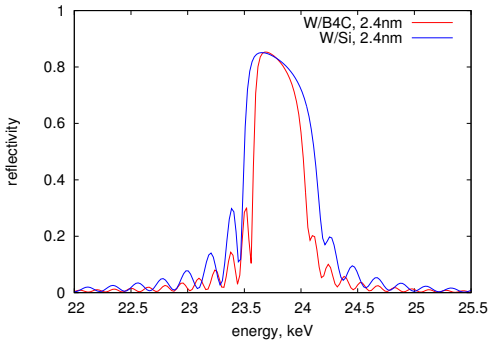

Figure 6: Comparison of the reflectivity curves for a mirror with two different multilayers: W/B4C (blue) and W/Si (red).

The reflectivity curve for different materials is given by the X-ray Oriented Program (XOP) [10]. The energy bandwidth increases as the thickness of the bilayer increases, but at the same time the Bragg angle θ_B decreases with the bi-layer thickness (see Fig. 7). Very shallow angles (in the order of 0.5deg) implies that the mirror length needs to be large to cover all the x-ray radiation, which in turn makes the structure more complex and expensive. For example, for an x-ray footprint with lateral size ΔL =3 mm and a Bragg angle of θ_B=0.5deg, the required monochromator length would be $\Delta L/\theta_B$ ~340 mm.

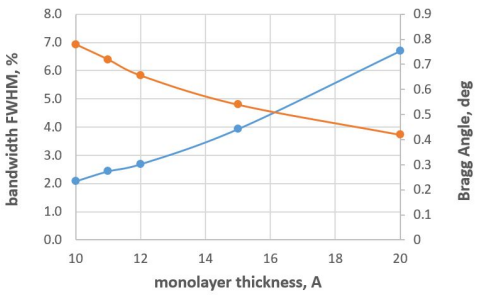

Figure 7: Bandwidth (in FWHM) and Bragg angle for a monochromator for different mono-layer thicness.

Finally, a good compromise is found for a 24 nm bilayer made of W/Si (with 12 nm for each monolayer of W and Si). Both W/Si and W/B4C offered similar results, and the final decision was based on economical costs. Its reflectivity curve is shown in Fig. 8, showing that the Bragg angle in the range of (20 - 30) keV varies between ~[0.5 - 0.75] deg. This is the final choice of monochromator, which is currently under construction. We note also that the monochromator is finally a single-crystal to again avoid long and expensive structures.

CONCLUSIONS

SRW simulations show that the most appropriate bandwidth for the monochromator in the proposed FE21 station is around 1%, which guarantees a good trade-off between the error produced by temporal coherence effects on the XH-

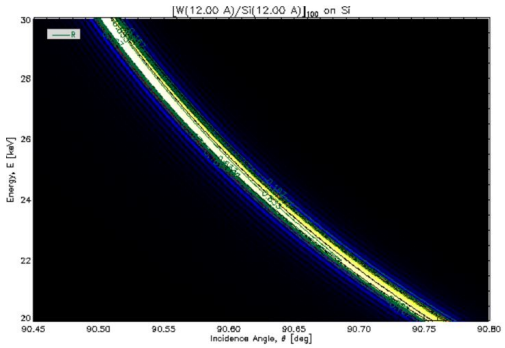

Figure 8: Reflectivity curve relating the peak energy and the Bragg angle for a monochromator of W/Si.

NFS technique (less than 1%) and the photon flux arriving to the detection station.

Using the XOP code, we have found that a single crystal monochromator of Si with a bi-layer 24 nm coating of W/Si fulfills the requirements set by the FE21 layout: energy peak of 23.7 keV, with a Bragg angle of θ_B=0.64 deg and a bandwidth of 1.2%. The expected photon energy range for the XHNFS experiments will be between (20-30) keV. The monochromator is currently under fabrication and it is expected to be delivered at the beginning of 2025.

REFERENCES

[1] U. Iriso, A. C. Cazorla, I. M. Solé, A. A. Nosych, and M. Zeus, "PSF Characterization of the ALBA X-Ray Pinholes", in *Proc. IBIC'22*, Kraków, Poland, pp. 421–425, 2022. doi:10.18429/JACoW-IBIC2022-WEP16

[2] M. Siano *et al.*, "Two-dimensional electron beam size measurements with x-ray heterodyne near field speckles", *Phys. Rev. Accel. Beams*, vol. 25, no. 5, p. 052 801, 2022. doi:10.1103/PhysRevAccelBeams.25.052801

[3] M. D. Alaimo *et al.*, "Probing the transverse coherence of an undulator x-ray beam using brownian particles", *Phys. Rev. Lett.*, vol. 103, no. 19, p. 194 805, 2009. doi:10.1103/PhysRevLett.103.194805

[4] Y. Kashyap, H. Wang, and K. Sawhney, "Two-dimensional transverse coherence measurement of hard-x-ray beams using near-field speckle", *Phys. Rev. A: At. Mol. Opt. Phys.*, vol. 92, no. 3, p. 033 842, 2015. doi:10.1103/PhysRevA.92.033842

[5] S. Mazzoni *et al.*, "Overview of the FCC-ee beam instrumentation R&D", presented at IBIC'24, Beijing, China, Sep. 2024, this conference.

[6] SRW, https://www.esrf.fr/Accelerators/Groups/InsertionDevices/Software/SRW

[7] M. Siano *et al.*, "Characterizing temporal coherence of visible synchrotron radiation with heterodyne near field speckles", *Phys. Rev. Accel. Beams*, vol. 20, no. 11, p. 110 702, 2017. doi:10.1103/PhysRevAccelBeams.20.110702

[8] M. Siano, B. Paroli, and M. A. C. Potenza, "Heterodyne near field speckles: From laser light to x-rays", *Adv. Phys.: X*, vol. 6, no. 1, p. 1 891 001, 2021. doi:10.1080/23746149.2021.1891001

ISBN: 978-3-95450-249-3 ISSN: 2673-5350 doi: 10.18429/JACoW-IBIC2024-TUP57

[9] J. Goodman, *Introduction to Fourier Optics*. Ben Roberts & Company, Englewood, Colorado, USA, 2007. doi:10.1063/1.3035549

[10] XOP, https://www.aps.anl.gov/Science/Scientific-Software/XOP